Specific features of thermal and magnetic properties of YbB_{50} at low temperatures

V. V. Novikov,[1,*] N. A. Zhemoedov,[1] A. V. Matovnikov,[1] N. V. Mitroshenkov,[1] E. A. Popova,[1] A. K. Tolstosheev,[2] B. Z. Malkin,[3] and S. L. Bud'ko[1,4]

[1]*Petrovsky Bryansk State University, Bezhitskaya 14, 241036 Bryansk, Russia*

[2]*Bryansk State Technical University, Boulevard 50-letiya Oktyabrya 7, 241035 Bryansk, Russia*

[3]*Kazan Federal University, Kremlevskaya 18, 420008 Kazan, Russia*

[4]*Ames Laboratory, US DOE and Department of Physics and Astronomy, Iowa State University, Ames, Iowa 50011, USA*

(Received 13 July 2017; revised manuscript received 15 February 2018; published 3 May 2018)

Heat capacity, thermal expansion, and magnetization of ytterbium boride YbB_{50} were studied at temperatures 0.6–300 K, 5–300 K, and 2–300 K, respectively. We revealed two smooth peaks at about 4.0 and 60 K in the temperature dependence of the heat capacity. A comparison with the heat capacity of the diamagnetic isostructural boride LuB_{50} shows that these anomalies can be attributed to excitations in the ytterbium sublattice (Schottky anomalies). A scheme for splitting of the ground $^2F_{7/2}$ multiplet of Yb^{3+} ions in the crystal field is proposed. Reliability of the proposed crystal-field energies of the Yb^{3+} ions is confirmed by the analysis of temperature dependencies of magnetic susceptibility and magnetization in applied magnetic fields up to 55 kOe. A clear anisotropy of the thermal expansion and a negative expansion within a wide temperature range (40–185 K) were observed. Assuming that this anomaly of the thermal expansion in higher borides is caused by the specific thermal evolution of a crystal lattice observed earlier, in particular, in LuB_{50}, and the interaction of rare-earth ions with lattice strains, we have determined phenomenological Grüneisen parameters which characterize effects due to thermal transitions of Yb^{3+} ions between the ground and excited states. A phase transition of YbB_{50} to any magnetically ordered state was not observed down to the lowest temperatures of experiments.

DOI: 10.1103/PhysRevMaterials.2.054401

I. INTRODUCTION

Rare-earth borides with the high content of boron RB_{12}, RB_{25}, RB_{50}, RB_{66}, where R stands for rare-earth metals, have been known and studied for several decades [1–5]. The most characteristic feature of the crystal structure of rare-earth high-boron-content compounds is the presence of B_{12} cluster in the boron sublattice. The high bond energy in the boron lattice of such compounds results in high melting point, hardness, acidity, and small compressibility values [6]. RB_{50} borides were the first rare-earth compounds with high boron content in which the unexpectedly strong magnetic interactions in the rare-earth subsystems were observed [7]. Whereas in the RB_{66} borides the transitions/crossovers into the magnetically ordered/spin-glass states were observed at temperatures about 1 K and below [8–10], magnetic susceptibilities of RB_{50} borides show clear maxima at temperatures of 2–18 K [7,11–13] caused by the antiferromagnetic interactions. The anomalies of RB_{50} heat capacity at low temperatures are characteristic smooth peaks (humps) of small amplitude which, according to the authors of Refs. [6,7], point to a certain degree of disorder or possibly short-range order of magnetic moments of rare-earth ions. The boron sublattice contains B_{12} icosahedral chains aligned along the c axis of the orthorhombic crystal lattice. Rare-earth ions form ladders along the c axis and are located inside the peanutlike large cavities in the boron sublattice. The location of boron atoms in the nearest surroundings of rare-earth ions is highly asymmetric. In particular, according to crystallographic data from Ref. [14], there are 16 boron atoms at the distances from 2.42 to 3.02 Å from each ytterbium ion in YbB_{50}. These atoms are distributed in such a way that 15 atoms are between the nearest-neighbor ytterbium ions along a ladder leg, but ten atoms are in the regions between these ytterbium dimers. This results in the ability of R^{3+} ions to take spatially close but energetically nonequivalent positions between which they can make transitions. The specific unstable dynamical systems formed this way result in anomalies in temperature dependencies of the heat capacity and the unit-cell volume [15].

The crystal-field (CF) impact on thermal properties of RB_{50} borides was found significant [11–13]. The CF contribution into the heat capacity $C_p(T)$ of rare-earth borides induces a broad anomaly of the Schottky type, but temperature dependencies of the lattice parameters $a(T)$, $b(T)$, $c(T)$ and the unit-cell volume $V(T)$ acquire quite a complex shape with wide temperature ranges of the negative expansion.

The latter fact can have a very important practical application, since varying the boride composition and forming solid solutions of different composition it is possible to get alloys with almost zero expansion within a wide temperature range [16].

By now, the peculiarities of thermal properties of RB_{50} borides for R = Tb, Dy, Ho, Er, Tm, Lu have been thoroughly studied [11–13,15,17,18]. The goal of the present paper is to analyze the properties of YbB_{50}.

II. EXPERIMENT

The YbB_{50} sample synthesis was accomplished by the metal reduction from its oxide similarly to other borides in its family

*Corresponding author: vvnovikov@mail.ru

 ©2018 American Physical Society

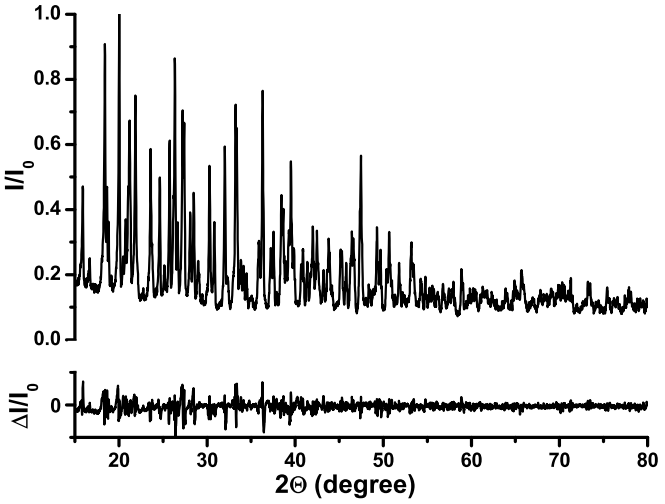

FIG. 1. Experimental x-ray-diffraction pattern of YbB_{50} and the difference between experimental data and scattering intensities calculated by PowderCell 2.3 program.

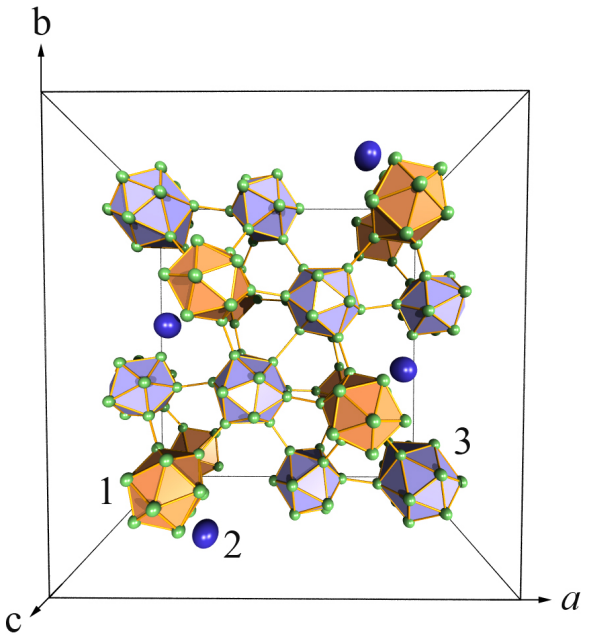

FIG. 2. The cross section of YbB_{50} structure in the ab plane with a slight inclination of the c axis. 1 and 2: polyhedrons B_{12}; 3: Yb atoms.

[11–13]. According to the chemical analysis, the composition of the synthesized sample corresponded to the formula of $YbB_{44.8}$. Hereafter, to denote the studied ytterbium boride sample, we will use the accustomed stoichiometry YbB_{50}. Naturally, all the calculations were performed using the real composition of our boride sample.

The crystal lattice parameters for YbB_{50} at 5–300 K $a(T)$, $b(T)$, $c(T)$ and the unit–cell volume $V(T) = a(T)b(T)c(T)$ were determined from Bragg diffraction angles for reflexes (450), (162), (254), measured by a DRON-7.0 x-ray diffractometer using the x-ray helium cryostat. The x-ray tube with the iron cathode was used [19–21]. The sample temperature was measured by "copper-copper +0.1% iron" thermocouple. The measurement accuracy was no lower than ±0.1 K. The x-ray diffraction analysis of the synthesized sample did not reveal any secondary phases. The angular positions of the peaks on the x-ray scattering pattern correspond to the data generated by the PowderCell 2.3 program for YbB_{50} structure (see Fig. 1).

The lattice parameters for the synthesized orthorhombic ytterbium boride with the space group *Pbam* at room temperature are a = 16.573 Å, $b = 17.587$ Å, $c = 9.4551$ Å. The error of the lattice parameters measurement was $\pm 10^{-4}$ Å. This error value was confirmed by the calibration measurements on the silicon sample [19]. As one could expect, these values are close to the data for the isostructural borosilicide $YbB_{45.6}Si_{1.0}$: $a = 16.636$ Å, $b = 17.644$ Å, $c = 9.488$ Å [22], and for the recently studied ytterbium boride $YbB_{43.3}$: $a = 16.5811$ Å, $b = 17.5950$ Å, $c = 9.4647$ Å [14]. The cross section of YbB_{50} structure in the ab plane is shown in Fig. 2.

The heat capacity of ytterbium boride was measured using the adiabatic vacuum calorimeter with periodic heating [23,24] at temperatures 2–300 K and a hybrid relaxation technique in a Quantum Design PPMS instrument with a He-3 option at temperatures between 0.5 and 30 K. The adiabatic conditions during the calorimetric experiments were provided by the system of screens surrounding the sample. The temperature of the screen closest to the sample was automatically maintained equal to the sample temperature accurate to ±0.0001 K. For this purpose, the ten-junction copper-copper +0.1% iron thermocouple was employed in the feedback circuit of the screen heat regulator. The sample temperature was measured by the standard germanium (1.5–20 K) and platinum (12–350 K) resistance thermometers. The inaccuracy of the measured molar heat capacity was less than 3% at 2–20 K, then it decreased to 1% at 60 K and remained within these values up to room temperature. These error limits were confirmed by the calibration measurements based on the sample of electrolyte copper having the purity of 99.996% which was melted and annealed in vacuum.

The magnetic susceptibility in the range of temperatures from 1.8 K up to 300 K in the applied magnetic field of 1 kOe and the field dependence of the low-temperature ($T = 1.8$ K) magnetization were measured using a Quantum Design MPMS-5 superconducting quantum interference device magnetometer.

III. RESULTS AND DISCUSSION

A. Heat capacity

The temperature dependence of heat capacity $C_p^-(T)$ for ytterbium boride YbB_{50} (Fig. 3) has the shape typical for RB_{50} compounds: there is a smooth peak at low temperature ($T_{max} \approx 4.16$ K), and close to linear dependence is observed at temperatures in the range 150–300 K. Since the studied boride is a semiconductor [22], it makes sense to review only the lattice (phonon) and magnetic (caused by $4f$ electrons localized at the Yb^{3+} ions) contributions to its heat capacity in the studied temperature range. To a first approximation, we assume that the lattice heat capacity of YbB_{50} is equal to the heat capacity $C_{LuB50}(T)$ of its isostructural diamagnetic counterpart LuB_{50} measured earlier and presented in Refs. [13,15]. Subtracting the values of $C_{LuB50}(T)$ from the measured heat capacity

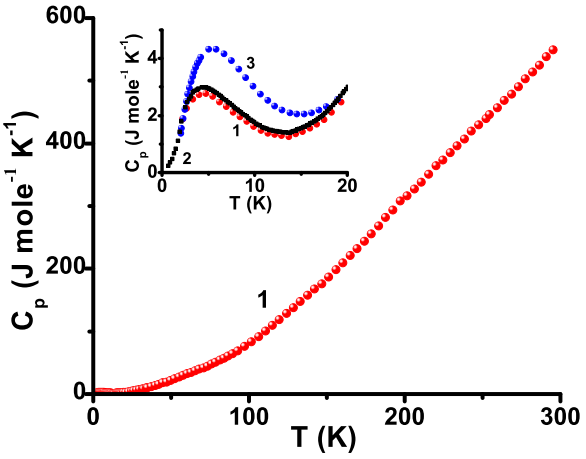

FIG. 3. Heat capacity of ytterbium borides. 1: YbB_{50} (2–300 K); 2: YbB_{50} (0.6–30 K); 3: $YbB_{45.6}Si_{1.0}$ [22].

$C_{YbB50}(T)$, we obtained the magnetic subsystem contribution $\Delta C(T)$ to the heat capacity of the ytterbium boride (Fig. 4). It should be noted that the entropy change connected with the magnetic contribution into the heat capacity,

$$\Delta S_m(T) = \int_{0.6}^{T} \frac{\Delta C(T)}{T} dT + R \ln 2 \qquad (1)$$

[the last term on the right-hand side of (1) is added to account for the Kramers degeneracy of energy levels of the Yb^{3+} ions in the absence of an external magnetic field; R is the gas constant] approaches $R \ln 8$ when T approaches room temperature. This value of ΔS_m corresponds to the degeneracy $2J + 1$ of the ground multiplet $^2F_{7/2}$ of the Yb^{3+} ions with the total angular momentum $J = 7/2$. So, the obtained temperature dependence of $\Delta C(T)$ can be interpreted in terms of thermal transitions between the CF sublevels of the ground multiplet of the Yb^{3+} ions. As it follows from negligible values of $\Delta C(T)$ for temperatures $T > 300$ K, the total splitting of the ground multiplet $^2F_{7/2}$ does not exceed 300 K, and we can neglect

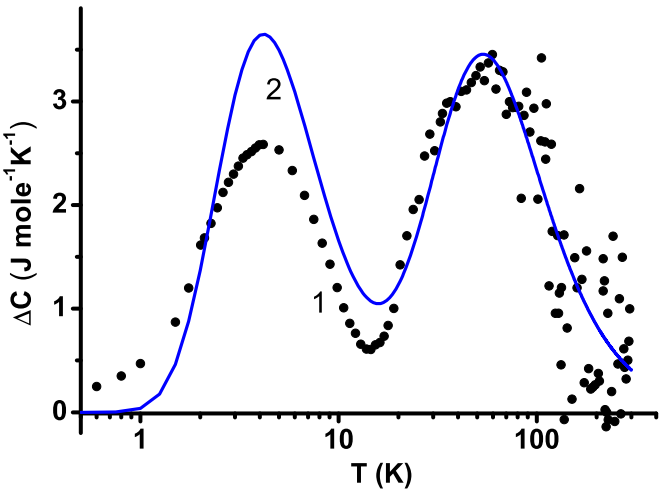

FIG. 4. The excess heat-capacity component of YbB_{50}. 1: experimental values of $\Delta C(T) = C_{YbB50}(T) - C_{LuB50}(T)$; 2: calculated temperature dependence of $C_R(T)$.

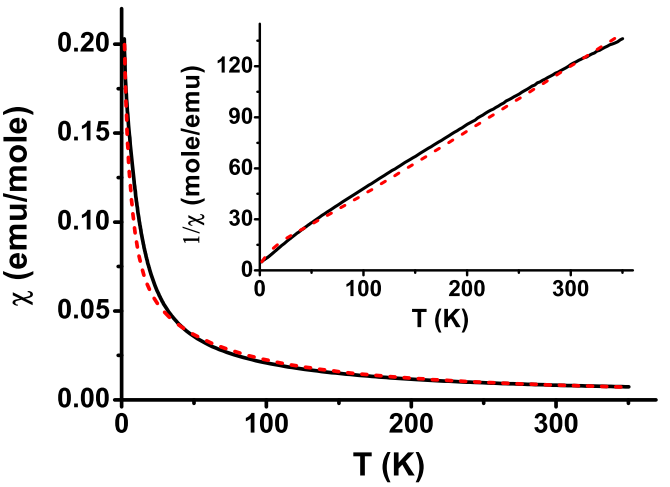

FIG. 5. Measured (solid lines) and simulated (dashed lines) temperature dependencies of the magnetic susceptibility of YbB_{50}. Inset: temperature dependence of the inverse magnetic susceptibility.

mixing of this multiplet with the excited one, $^2F_{5/2}$, in the crystal field because the corresponding energy gap due to the spin-orbit coupling exceeds 10^4 K [$E(^2F_{5/2}) - E(^2F_{7/2}) = 7\zeta/2$, where $\zeta = 4270$ K is the spin-orbit coupling constant [25]].

B. Magnetic properties

Figure 5 features the temperature dependence of the magnetic dc susceptibility of YbB_{50}. It should be noted that the raw data for $\chi(T) = M(T)/B$ obtained from measurements of magnetization M in the field $B = 1$ kOe were corrected by subtracting a small (but comparable to the susceptibility value at room temperature) almost independent on temperature positive contribution of unknown nature that was revealed also in our measurements of the susceptibility of the LuB_{50} sample synthesized in similar conditions and in Ref. [26] for different rare-earth borosilicides. The low-temperature part of the renormalized susceptibility is close to the data presented in Refs. [22,26] for the pseudoisostructural $YbB_{45.6}Si_{1.0}$.

In the temperature range from 50 to 300 K the inverse susceptibility can be well approximated by the Curie-Weiss behavior (see inset in Fig. 5) with the negative Curie-Weiss temperature $\theta = -22$ K and the effective magnetic moment of 4.55 μ_B that is close to the magnetic moment 4.535 μ_B of a free Yb^{3+} ion.

The measured field dependence of the magnetization of YbB_{50} polycrystalline sample at a temperature of 1.8 K is presented in Fig. 6. The monotonous increase of the magnetization with the field strength does not show any anomalies, and only a weak tendency to saturation becomes noticeable at the highest fields above 50 kOe.

Rare-earth ions occupy the Wyckoff 8*i* positions in the *Pbam* structure and have the same energy spectra in zero magnetic field. There are four magnetically nonequivalent pairs of R^{3+} ions in the unit cell with coordinates $\pm(x,y,z)$, $\pm(x,y,-z)$, $\pm(x+1/2,1/2-y,z)$, $\pm(x+1/2,1/2-y,-z)$ in the crystallographic Cartesian system of coordinates, however, all R^{3+} ions are equivalent in the magnetic fields

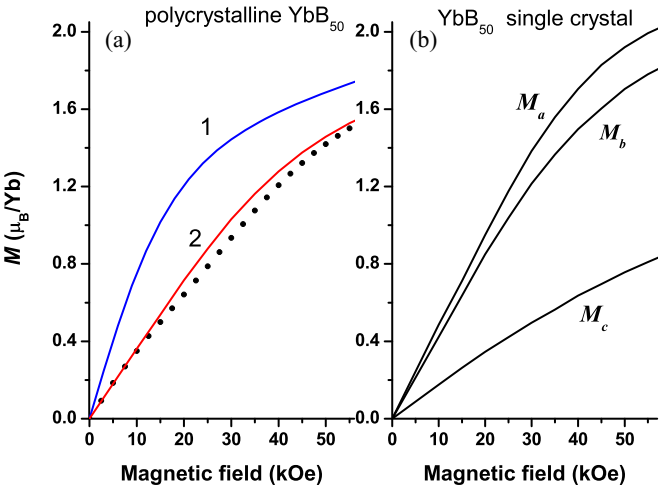

FIG. 6. (a) Measured (symbols) and simulated (solid lines) field dependencies of the magnetization of YbB_{50} polycrystalline sample. 1: magnetic moment of a single Yb^{3+} ion averaged over the applied field directions along the crystallographic a, b, and c axes; 2: the renormalized magnetic moment in the frameworks of the molecular field approximation. (b) Simulated magnetization of YbB_{50} single crystal in magnetic fields directed along the a, b, and c axes. $T = 1.8$ K.

directed along the crystallographic axes. Below, for simplicity, we use the same effective single-ion Hamiltonian for all rare-earth ions in the sample assuming that an applied magnetic field $\boldsymbol{B}$ is parallel to one of the crystallographic axes.

Considering magnetic interactions between rare-earth ions in the frameworks of the mean-field approximation, we can write the effective Hamiltonian operating in the space of states of the ground multiplet $^2F_{7/2}$ of an Yb^{3+} ion as follows: $H = H_0 + H_{\text{el-def}}$, $H_0 = H_{\text{CF}} + H_Z$. Here

$$H_{\text{CF}} = \sum_{p=2,4,6} \sum_{k=-p}^{p} a_p B_p^k O_p^k \ (a_2 = \alpha_J,\ a_4 = \beta_J,\ a_6 = \gamma_J) \tag{2}$$

is the CF Hamiltonian (O_p^k are the Stevens operators with the corresponding reduced matrix elements a_p [25], B_p^k are the CF parameters), the Zeeman interaction with the local magnetic field $\boldsymbol{B}_{\text{loc}} = \boldsymbol{B} + \boldsymbol{\lambda} \cdot \boldsymbol{M}$ ($\boldsymbol{M}$ is the magnetization, and $\boldsymbol{\lambda}$ is the molecular field tensor) is represented by the operator $H_Z = g_J \mu_B \boldsymbol{J} \cdot \boldsymbol{B}_{\text{loc}}$ (μ_B is the Bohr magneton, $g_J = 8/7$ is the Landé factor), and the linear interaction of a rare-earth ion with the lattice strains defined by the deformation tensor $\boldsymbol{e}$ is represented by the operator $H_{\text{el-def}} = \sum_{\alpha\beta} Q_{\alpha\beta} e_{\alpha\beta}$ (electronic operators $Q_{\alpha\beta}$ can be presented as linear combinations of the Stevens operators similarly to H_{CF}). Below we consider the electron-deformation interaction as a perturbation. Different physical properties of the equilibrium rare-earth subsystem can be described using a free energy $F_R(T, \boldsymbol{B}, \boldsymbol{e}) = -N k_B T \ln Z$ where k_B stands for the Boltzmann constant, N is the number of the Yb^{3+} ions per unit volume, and $Z = \text{Tr}[\exp(-H/k_B T)]$ is the partition function. In particular, the heat capacity $C_R = -\partial^2 F_R / \partial T^2$ is given by the expression

$$C_R(T) = \frac{N}{k_B T^2} \left[\langle H_0^2 \rangle - \langle H_0 \rangle^2 \right], \tag{3}$$

where angular brackets mean quantum-statistical averaging, $\langle A \rangle = \text{Tr}[A \exp(-H_0/k_B T)]/Z_0$, and $Z_0 = \sum_i \exp[-E_i(\boldsymbol{B})/k_B T]$, where $E_i(\boldsymbol{B})$ are the eigenvalues of the Hamiltonian H_0. Similarly, we can obtain the following expression for the magnetization $\boldsymbol{M} = -\nabla_{\boldsymbol{B}} F_R$:

$$\boldsymbol{M}(\boldsymbol{B}_{\text{loc}}) = -N \langle g_J \mu_B \boldsymbol{J} \rangle. \tag{4}$$

The magnetization dependence on the external field $\boldsymbol{M}(\boldsymbol{B})$ is determined by the self-consistent equation $\boldsymbol{B}_{\text{loc}}(\boldsymbol{M}) = \boldsymbol{B} + \lambda \boldsymbol{M}$ where the nonlinear function $\boldsymbol{B}_{\text{loc}}(\boldsymbol{M})$ stands for the inverse function (4).

The relative change of the system volume is determined by the trace of a deformation tensor. So, to find the coefficient of volume thermal expansion $\beta_R = \partial \text{Tr}(\boldsymbol{e})/\partial T$ induced by the electron-deformation interaction, we can use the minimum condition for the total free energy of the crystal $F = F_{\text{el}} + N \langle H_{\text{el-def}} \rangle$ that involves the elastic energy $F_{\text{el}} = \sum_{\alpha\beta\gamma\delta} C_{\alpha\beta\gamma\delta} e_{\alpha\beta} e_{\gamma\delta}/2$ ($C_{\alpha\beta\gamma\delta}$ are the elastic constants) along with the strain dependent terms in the free energy of the rare-earth subsystem. Using the linear transformation in the space of elastic tensor components, we can single out the term $Q_0 \text{Tr}(\boldsymbol{e})$ in $H_{\text{el-def}}$ and obtain the following relative volume change:

$$\text{Tr}(e) = -\kappa N \langle Q_0 \rangle, \tag{5}$$

where κ stands for the isothermal compressibility. The coefficient of volume expansion takes the form

$$\beta_R(T) = -N\kappa \frac{\partial}{\partial T} \langle Q_0 \rangle = -\frac{N\kappa}{k_B T^2} [\langle H_0 Q_0 \rangle - \langle H_0 \rangle \langle Q_0 \rangle]. \tag{6}$$

Only relative shifts of the energy levels are of importance, and we denote differences of the diagonal matrix elements of the operator Q_0 in the basis of the eigenfunctions $|i\rangle$ of the Hamiltonian H_0 corresponding to energies E_i as follows (here $i = 0$ refers to the ground state):

$$\gamma_i = -(\langle i|Q_0|i\rangle - \langle 0|Q_0|0\rangle)/(E_i - E_0). \tag{7}$$

By analogy with the Grüneisen parameters of phonon modes in crystals, the quantities defined in (7), $\gamma_i = -\partial \ln(E_i - E_0)/\partial \ln V$, can be called CF Grüneisen parameters [27]. The explicit dependence of the coefficient of volume expansion on parameters γ_i is presented below [28]:

$$\beta_R(T) = \frac{N\kappa}{k_B T^2 Z_0} \sum_i \gamma_i (E_i - E_0)(E_i - \langle H_0 \rangle) \exp\left(-\frac{E_i}{k_B T}\right). \tag{8}$$

In orthorhombic higher borides RB_{50}, there are no symmetry related restrictions on values of the CF parameters or any relations between their values. However, it makes no sense to work with the total set of 27 unknown CF parameters.

The low-temperature Schottky anomaly in the heat capacity (Fig. 4) evidences two closely spaced Kramers doublets as the lowest sublevels of the $^2F_{7/2}$ multiplet of Yb^{3+} ions. This quasiquadruplet CF state indicates the dominant role of the qubic component of the crystal field that splits a multplet with the angular momentum $J = 7/2$ into two doublets Γ_6, Γ_7 and a quadruplet Γ_8. Thus, to describe the experimental data, we introduced, as the first approximation, a model operating with seven CF parameters B_p^k which determine the cubic (B_4^4, B_6^4), axial (along the C_4 cubic axis, B_2^0, B_4^0, B_6^0) and rhombic (B_2^2, B_2^{-2}) CF components in the crystallographic system of coordinates ($\boldsymbol{x} \parallel \boldsymbol{a}$, $\boldsymbol{y} \parallel \boldsymbol{b}$, $\boldsymbol{z} \parallel \boldsymbol{c}$). Small values of the rhombic quadrupole field parameters (they are introduced to account for possible magnetic anisotropy in the ab plane and practically do not affect the values of other model parameters given below) were fixed, $[(B_2^2)^2 + (B_2^{-2})^2]^{1/2} = 8$ K. The five parameters of the cubic and axial CF components were varied along with the molecular field constant (for simplicity, the molecular field tensor was approximated by a scalar λ) to fit the measured temperature dependence of the heat capacity $\Delta C(T)$ and the field dependence of the magnetization. For a given set of CF parameters, the heat capacity of the Yb^{3+} ions was calculated according to (3) using numerical diagonalization of the Hamiltonian H_{CF}. Similarly, the magnetic moments of the Yb^{3+} ions at 1.8 K were calculated versus local magnetic fields directed along the mutually orthogonal crystallographic axes according to (4) using numerical diagonalization of the Hamiltonian H_0. Then, for a given value of the parameter λ, the self-consistent dependencies of the single-ion moments m_α ($\alpha = a,b,c$) on the external field B_α were obtained from graphical solutions of the equations $B_{\mathrm{loc},\alpha}(m_\alpha) = B_\alpha + 8\lambda m_\alpha / V$ (here V is the unit-cell volume containing eight rare-earth ions). The averaged values of the magnetic moments, $\sum_{\alpha=a,b,c} m_\alpha/3$, were compared with the measured magnetization of the polycrystalline sample.

From the fitting procedure, we obtained the following values of the model parameters: $B_2^0 = 7.3$, $B_4^0 = -9.4$, $B_6^0 = -24.6$, $B_4^4 = -31.9$, $B_6^4 = 467$ (K), and $8\lambda\mu_B/V = -12$ kOe. The corresponding energies of the CF sublevels of the ground multiplet of the Yb^{3+} ions in the zero magnetic field are 0, 10.4, 106.0, and 166.7 (in degrees Kelvin). The corresponding temperature dependence of the heat capacity $C_R(T)$ agrees satisfactorily with the measured excess contribution of the Yb^{3+} ions $\Delta C(T)$ (see Fig. 4). A higher intensity of the calculated low-temperature peak can be explained as a result of broadening and a corresponding suppression of the Schottky anomaly due to magnetic interactions and random lattice strains which are expected to be rather strong in real RB_{50} crystals containing a number of boron vacancies.

The calculated susceptibility $\chi_0(T) = (\chi_{aa} + \chi_{bb} + \chi_{cc})/3$ of an isolated Yb^{3+} in the crystal field (here $\chi_{\alpha\beta}$ are components of the single-ion susceptibility tensor) is much greater (about three times more) than the measured susceptibility of the polycrystalline YbB_{50} sample in the low-temperature region. This provides evidence for strong suppression of the responses of the ytterbium subsystem on external magnetic fields due to antiferromagnetic interactions between the Kramers' rare-earth ions. An introduction of the molecular field leads to the renormalization of the single-ion susceptibilities, and the susceptibility of a polycrystalline sample takes the following form (per mole):

$$\chi_R(T) = N_A \sum_{\alpha=a,b,c} \frac{\chi_{\alpha\alpha}(T)}{3(1 - 8\lambda\chi_{\alpha\alpha}/V)}, \tag{9}$$

where N_A is the Avogadro number. As is seen in Fig. 5, the calculated susceptibility $\chi_R(T)$ matches well the experimental data in the total range of available temperatures.

Assuming the Heisenberg isotropic exchange interactions between ytterbium ions with total spin S ($H_{\mathrm{exch}} = -J_{\mathrm{ex}}\boldsymbol{S}_1\boldsymbol{S}_2$), we can connect the molecular-field constant λ introduced above with the exchange integrals J_{ex}, $\lambda = V[(g_J - 1)/g_J]^2 \sum J_{\mathrm{ex}}/8\mu_B^2$, where the sum is taken over neighbors of an ytterbium ion. The value of λ used in simulations of the susceptibility corresponds to rather large exchange energy of $\sum J_{\mathrm{ex}} = -50$ K. As far as we know, the largest exchange integral for a ytterbium dimer in ionic compound $Cs_3Yb_2Br_9$, $J_{\mathrm{ex}} = -3.65$ K, was found in Ref. [29]. Nevertheless, we had to introduce such strong antiferromagnetic correlations to reproduce satisfactorily the measured magnetization of YbB_{50} at low temperatures [see Fig. 6(a)].

As is seen in Fig. 6(b), the derived CF model brings remarkable magnetic anisotropy of the XY type of the Yb^{3+} ions in the ground state; this agrees qualitatively with the measured low-temperature field dependence of the magnetization of the $YbB_{45.6}Si_{1.0}$ crystal [22].

C. Lattice dynamics

A distinct anisotropy of thermal expansion was revealed from temperature dependences of the lattice parameters and the unit-cell volume of YbB_{50} (Fig. 7). The negative thermal expansion along the a and b axes in wide temperature regions of 5–150 K and 120–300 K, respectively, as well as close to zero expansion along the c axis, should be noted. We can compare temperature variations of the unit-cell volumes of YbB_{50} [$V_{\mathrm{YbB50}}(T)$] and the diamagnetic boride LuB_{50} [$V_{\mathrm{LuB50}}(T)$] [13,15]. Assuming to the first approximation that the lattice contributions $V_{\mathrm{lat}}(T)$ to the volume expansion of these isostructural borides are the same, we have done the following: the $V_{\mathrm{LuB50}}(T)$ curve was moved by means of parallel shift in the direction of the Y axis up to its contact with the $V_{\mathrm{YbB50}}(T)$ dependence at the lowest temperatures of the experiment (at about 5 K). We suppose that $V_{\mathrm{lat}}(T)$ equals the obtained new dependence $V^*_{\mathrm{LuB50}}(T)$, and the difference $\Delta V(T) = V_{\mathrm{YbB50}}(T) - V^*_{\mathrm{LuB50}}(T)$ (Fig. 8, curve 1) is caused, in our opinion, by the interaction of the ytterbium subsystem (namely, localized $4f$ electrons) with the lattice strains. The reliability of this assumption is confirmed by clear correlations between the positions of the Schottky anomalies in the heat capacity and the extremum temperatures in the temperature dependence of the coefficient of volume expansion $\Delta\beta(T) = (1/\Delta V)d(\Delta V)/dT$ presented by curve 2 in Fig. 8.

Using the expression (8) and values of γ_i as fitting parameters, we calculated the temperature dependence of the volume thermal expansion $\beta_R(T)$ for YbB_{50} (curve 3 in Fig. 8). The satisfactory correspondence between the experimental $\Delta\beta(T)$ and estimated $\beta_R(T)$ dependencies was achieved with the following Grüneisen parameters: $\gamma_1 = 42$, $\gamma_2 = 65$, $\gamma_3 = -128$. Such large absolute values of Grüneisen parameters are characteristic of the CF effect on the thermal expansion of

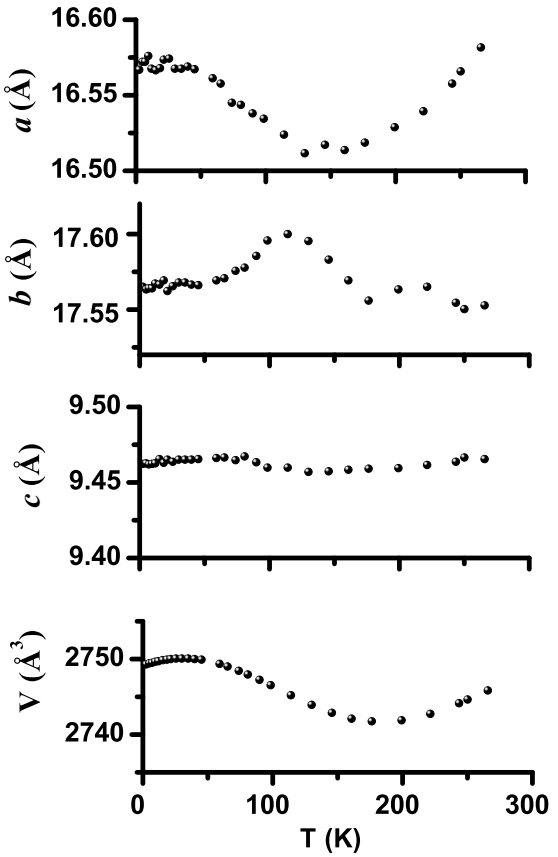

FIG. 7. Temperature dependencies of the lattice parameters and unit-cell volume of YbB_{50}.

rare-earth borides [11–13,15,17,18]. Note that similar values of Grüneisen parameters were obtained in the studies of thermal-expansion coefficients for alkali halides containing noncenter ions [30]; it is possible that anomalies in thermal expansion of rare-earth borides are caused by strong coupling between electronic and lattice degrees of freedom corresponding to CF excitations and tunneling of rare-earth ions in peanut cages in the boron sublattice, respectively.

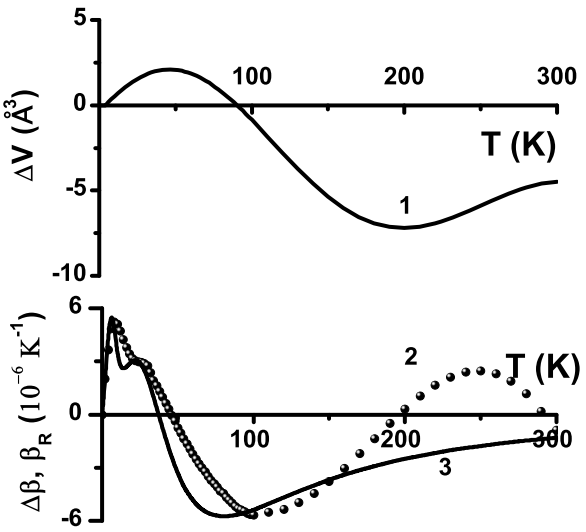

FIG. 8. The temperature dependence of the difference between the unit-cell volumes of YbB_{50} and LuB_{50}, $\Delta V = V_{YbB50}(T) - V^*_{LuB50}(T)$ (1), and the anomalies in the thermal-expansion coefficients $\Delta\beta$ (2) and β_R (3) of YbB_{50}.

IV. CONCLUSION

The comprehensive study of the YbB_{50} thermal and magnetic properties within the wide range of temperatures made it possible to reveal the anomalies in the studied properties, caused by the specific boride crystal structure as well as the antiferromagnetic interactions in its magnetic subsystem.

It is found that the crystal-field impact on the YbB_{50} thermal and magnetic properties is significant. The prominent anomalies in heat capacity, thermal expansion, and magnetic properties were satisfactorily described by the CF model. Analysis of the measured temperature dependence of the heat capacity from 0.6 K up to room temperature and of the low-temperature magnetic properties did not reveal anomalies that could be attributed to magnetic ordering processes (transition to antiferromagnetic phase) or to the formation of a spin-glass state. An analysis of the magnetic susceptibility and magnetization of YbB_{50} in the studied temperature range made it possible to obtain values of the parameters of the crystal field, and confirmed the reliability of the results of a joint calorimetric and x-ray-scattering studies of the low-temperature thermal properties. The peculiar behavior of the lattice constants $a(T)$, $b(T)$, $c(T)$ and the unit-cell volume $V(T)$ dependencies containing wide regions of almost zero or negative expansion should be also noted. These peculiarities of YbB_{50} thermal expansion are of significant interest both from a scientific and a practical point of view.

The microscopic model is derived that allowed us to reproduce successfully the experimental data. The distinguishing feature of this model is the dominant cubic component of the crystal field defined by the six-rank spherical tensor operators and the strong suppression of the quadrupole and hexadecapole components. It is well known that the sets of CF parameters of rare-earth ions in isomorphic compounds are reliable if they vary monotonously along the lanthanide series. Our preliminary results of simulations of thermodynamic and magnetic properties of TmB_{50} and ErB_{50} (thulium and erbium are the nearest and the next-nearest neighbors of ytterbium, respectively) by making use of the parameters obtained in the present work confirm the validity of the proposed CF model. The calculated energy patterns, in particular, the quasitriplet and the quasiquadruplet as the ground states of Tm^{3+} and Er^{3+} ions, respectively, and the corresponding magnetic characteristics are consistent, at least qualitatively, with the available experimental data [11,12,26].

However, obviously, it is necessary to conduct the experiments on neutron diffraction for clear understanding of what is occurring in magnetic subsystems of higher borides RB_{50} as the temperature decreases.

ACKNOWLEDGMENTS

The research was fulfilled under the auspices of the Russian Science Foundation (Project No. 16-12-00004). The authors are grateful to the anonymous referee for useful comments.

[1] V. I. Matkovich, R. F. Giese, and J. Economy, Z. Kristallogr. **122**, 116 (1965).

[2] J. L. Hord and R. E. Hughes, in *The Chemistry of Boron and its Compounds*, edited by E. L. Muetterties (Wiley, New York, 1967).

[3] R. Naslain, A. Guette, and P. Hagenmuller, J. Less Common Met. **47**, 1 (1976).

[4] O. A. Golikova, Phys. Status Solidi **101**, 277 (1987).

[5] D. Emin, J. Solid State Chem. **177**, 1619 (2004).

[6] T. Mori, Handb. Phys. Chem. Rare Earths **38**, 105 (2008).

[7] T. Mori and T. Tanaka, J. Phys. Soc. Jpn. **69**, 579 (2000).

[8] K. Flachbart, S. Gabani, T. Mori, and K. Siemensmeyer, Acta Phys. Pol. A **118**, 875 (2010).

[9] V. V. Novikov, D. V. Avdashchenko, A. V. Matovnikov, N. V. Moiseev, S. L. Bud'ko, and T. Tanaka, Physica B: Condens. Matter **406**, 2642 (2011).

[10] V. V. Novikov, D. V. Avdashchenko, S. L. Bud'Ko, N. V. Mitroshenkov, A. V. Matovnikov, H. Kim, M. A. Tanatar, and R. Prozorov, Philos. Mag. **93**, 1110 (2013).

[11] V. V. Novikov, N. A. Zhemoedov, A. V. Matovnikov, N. V. Mitroshenkov, B. G. Ueland, and S. L. Bud'ko, J. Alloys Compd. **684**, 714 (2016).

[12] V. V. Novikov, N. A. Zhemoedov, N. V. Mitroshenkov, and A. V. Matovnikov, Dalton Trans. **45**, 17447 (2016).

[13] V. V. Novikov, N. A. Zhemoedov, A. V. Matovnikov, N. V. Mitroshenkov, B. I. Kornev, S. V. Kuznetsov, E. A. Popova, B. G. Ueland, S. L. Bud'ko, and A. K. Tolstosheev, J. Therm. Anal. Calorim. **129**, 15 (2017).

[14] O. Sologub, L. P. Salamakha, B. Stöger, P. F. Rogl, T. Mori, G. Eguchi, H. Michor, and E. Bauer, J. Solid State Chem. **255**, 172 (2017).

[15] V. V. Novikov, N. A. Zhemoedov, A. V. Matovnikov, N. V. Mitroshenkov, S. V. Kuznetsov, and S. L. Bud'ko, Dalton Trans. **44**, 15865 (2015).

[16] J. N. Grima, V. Zammit, and R. Gatt, Xjenza **11**, 17 (2006).

[17] V. V. Novikov, N. A. Zhemoedov, A. V. Matovnikov, N. V. Mitroshenkov, S. V. Kuznetsov, and S. L Bud'ko, J. Magn. Magn. Mater. **449**, 257 (2018).

[18] V. V. Novikov, N. A. Zhemoedov, A. V. Matovnikov, N. V. Mitroshenkov, S. V. Kuznetsov, and S. L. Bud'ko, J. Alloys Compd. **724**, 782 (2017)

[19] V. V. Novikov, N. V. Mitroshenkov, A. V. Matovnikov, D. V. Avdashchenko, S. V. Trubnickov, and A. V. Morozov, J. Therm. Anal. Calorim. **120**, 1597 (2015).

[20] V. V. Novikov, A. V. Matovnikov, T. A. Chukina, A. A. Sidorov, and E. A. Kul'chenkov, Phys. Solid State **49**, 2034 (2007).

[21] V. V. Novikov, A. V. Matovnikov, N. V. Mitroshenkov, and A. V. Shevelkov, J. Alloys Compd. **684**, 564 (2016).

[22] T. Mori and T. Tanaka, J. Alloys Compd. **348**, 203 (2003).

[23] N. N. Sirota, A. M. Antjukhov, V. V. Novikov, and V. A. Fjodorov, Cryst. Res. Technol. **17**, 279 (1982).

[24] N. N. Sirota, V. V. Novikov, and A. M. Antjukhov, Russian J. Phys. Chem. A **57**, 542 (1983).

[25] A. Abragam and B. Bleaney, *Electron Paramagnetic Resonance of Transition ions* (Clarendon, Oxford, 1970).

[26] T. Mori, Z. Kristallogr. **221**, 464 (2006).

[27] A. Tari, *The Heat Capacity of Matter at Low Temperatures* (Imperial College Press, London, 2003).

[28] H. R. Ott and B. Lüthi, Phys. Rev. Lett. **36**, 600 (1976).

[29] R. L. Carlin, K. E. Merabet, and D. P. Shum, J. Appl. Phys. **67**, 5855 (1990).

[30] C. R. Case, K. O. McLean, C. A. Swenson, and G. K. White, in *Proceedings of the 1971 Thermal Expansion Symposium*, edited by H. C. Wolfe, M. G. Graham, and H. E. Hagy, AIP Conf. Proc. No. 3 (AIP, New York,1972), p. 183.